A novel metamorphic mechanism for efficient additive manufacturing of components with variable wall thickness

Yang Xie[a], Haiou Zhang[*a], Guilan Wang[b], Fei Zhou[a]

[a]State Key Laboratory of Digital Manufacturing Equipment and Technology, Huazhong University of Science and Technology, Wuhan 430074, PR China

[b]State Key Laboratory of Materials Processing and Die & Mould Technology, Huazhong University of Science and Technology, Wuhan 430074, PR China

REVIEWED

Abstract

A novel metamorphic rolling mechanism (MRM) based on genetic evolution synthesis that realized multiway, multiple-DOF and synchronous plastic forming in arc based deposition processing of components with variable wall thickness is proposed in this paper. Topology and mechanical structure of the metamorphic mechanism is presented and D-H equation is derived. Experiments show that firstly efficient manufacturing of components with variable wall thickness can be realized by synchronous rolling in vertical direction. Secondly precision and surface configurations of the components are improved compared with that of freeform deposition manufacturing. The metamorphic mechanism provides possibilities of efficient hybrid manufacturing of near net shape components with variable wall thickness.

Introduction

Metamorphic mechanism [1] started to be investigated in 1996 and its concept was proposed in 1998 by Dai [2]. In contrast to traditional mechanism, metamorphic mechanism has different configurations and its topology and mobility change as it moves from one configuration to another. Metamorphic mechanism can achieve different working behavior by their multiple configurations, variable topology and changeable mobility [3]. Metamorphic Rolling mechanism was first introduced to assist additive manufacturing in 2013 by Zhang [4]. The metamorphic rolling mechanism was designed and applied for reducing the cumulative error in the Z-direction [5].

Arc based deposition processing [6-8] of components is more efficiency and low-cost [9] than other additive manufacturing processing using laser [10] or electron beam [11] as energy source, which provides an advantageous alternative to inexpensive access of additive manufacturing technology and shows great commercial potential for 3D printing. To control the surface precision of the overlapping beads [12], geometry of bead is analyzed [13-15] and the top surface will conventionally be milled after deposition of each layer [16, 17]. But the material utilization rate is low and the processing cycle is extended.

*Corresponding author E-mail: zholab@mail.hust.edu.cn (Haiou Zhang). wgllab@mail.hust.edu.cn.

In this paper, a novel metamorphic rolling mechanism was designed through a first proposed genetic evolution synthesis operator. Topology and mechanical structure of the metamorphic mechanism is presented and D-H equation is derived. Experiments of efficient manufacturing of components with variable wall thickness realized by synchronous compressing in vertical direction [18] was carried out. Precision, and surface configurations of the components were measured compared with that of freeform deposition manufacturing. Results show that the metamorphic mechanism provides possibilities of hybrid manufacturing of near net shape components with variable wall thickness efficiently.

Design of metamorphic rolling mechanism

1. Working phases of metamorphic rolling mechanism.

A metamorphic mechanism is a variable topology mechanism that can be evolved into a set of traditional mechanism, which function as multiple working-phase mechanisms, realizing multiple working state configurations for multiple kinematic functions[]. Each working-phase mechanism has one degree of freedom (DOF). According to the working condition, metamorphic mechanism can change from one working-phase mechanism to another. The vertical rolls have three working phases:

1) Two vertical rolls both work. It is most often used in deposition of single bead or thin-wall components. And the distance between two rolls can be changed to manufacture components with variable wall thickness.

2) One vertical roll works and the other rises from working position. It is used for outer edges of multi-bended parts or when there is interference at one working position.

3) Two vertical rolls both rise from working position. It is used in the deposition of root beads close to substrate.

Thus the source-metamorphic rolling mechanism should have 2 DOF, one translation DOF P and one rotation DOF R, to achieve the above 3 working phases.

2. A first proposed genetic evolution synthesis operator.

A genetic evolution synthesis operator $\bigcup^{X}$ was first proposed as follows:

$$b_i \bigcup^{X} b_j = b_i A_m A_n \ldots b_j = {}^{X}M \tag{1}$$

This operation results in a working-phase mechanism ${}^{X}M$ from source kinematic pair b_i and executive kinematic pair ${}^{b}j$ by multiplying a combination of transmission genes which satisfied non-genovariation evolution between adjacent genes. Any combination can get a theoretically feasible working-phase mechanism. Taking consideration of mechanism flexibility and number of unnecessary transmission parts and DOF, the optimal mechanism should have two characteristics as follows:

1) The number of unnecessary genes should be few, better no more than 3, to

make working-phase mechanism simple and perform well.

2) DOF of working-phase mechanism should be 1. If the DOF of genetic combination is more than 1, External constraint should be added to ensure the uniqueness of executive gene.

3. Topology and mechanical principle diagrams of the working-phase mechanisms and source-metamorphic mechanism.

Considering motor drives screw to provide power source, substitute P for the source kinematic pair b_i and the 2 DOF R and P of the source-metamorphic rolling mechanism for the executive kinematic pair ${}^{b}_{j}$ in Eq. (1), the working-phase mechanisms ${}^{1}M$ and ${}^{2}M$ can be expressed as:

$$P\bigcup {}^{X}R = P\Pi R - R - R - R = a_6 a_1 A_1 = [a_6; a_1 A_1; a_f] = {}^{1}M \tag{2}$$

$$P\bigcup {}^{X}P = P\Pi R - R\Pi P = a_6 A_2 = [a_6; A_2; a_f] = {}^{2}M \tag{3}$$

The generation of the source-metamorphic mechanism ${}^{S}M$ from the genetic evolution synthesis can be expressed as Eq. (4).

$$\begin{aligned} {}^{S}M &= {}^{1}M\bigcup {}^{2}M = [a_6; a_1 A_1; a_f]\bigcup [a_6; A_2; a_f] \\ &= [(a_6 \oplus a_1); (a_1 A_1\bigcup a_6\bigcup A_2 \backslash a_1); (a_f \bigcup a_f)] \\ &= [a_6, a_1; (a_1 A_1\bigcup a_6\bigcup a_5); a_f] \\ &= [a_6, a_1; a_1 A_1; a_f] = P\Pi R - R - R - R - R\Pi P \end{aligned} \tag{4}$$

From the biological topologies expressed in Eq. (4) to Eq. (6), mechanical principle diagrams of the working-phase mechanisms and source-metamorphic mechanism can be established, shown in Fig.1.

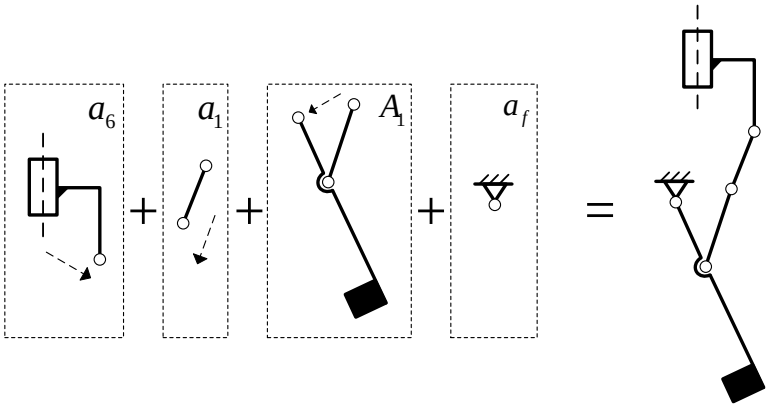

(a)

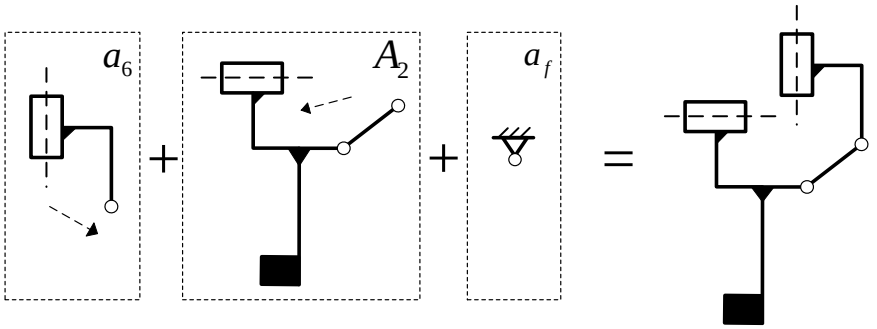

(b)

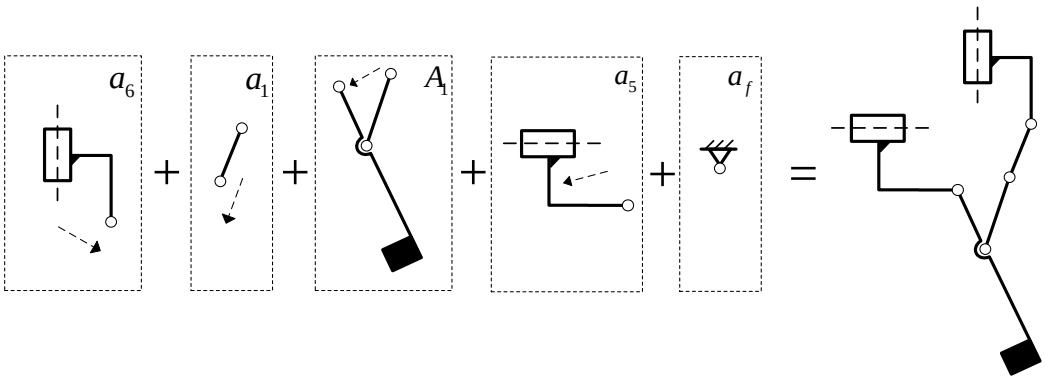

(c)

Fig.1. Mechanical principle diagrams of the working-phase mechanisms (a, b) and source-metamorphic mechanism (c).

The DOF of the first working-phase mechanism is 2. Constraint is added to reduce redundant DOF and ensure the metamorphic process as shown in Fig.2. Reducing redundant DOF makes the followers of metamorphic rolling mechanism a local four-bar linkage mechanism. In addition, the rigidity of the metamorphic mechanism is improved by taking use of the locking-position characteristic of four-bar linkage mechanism.

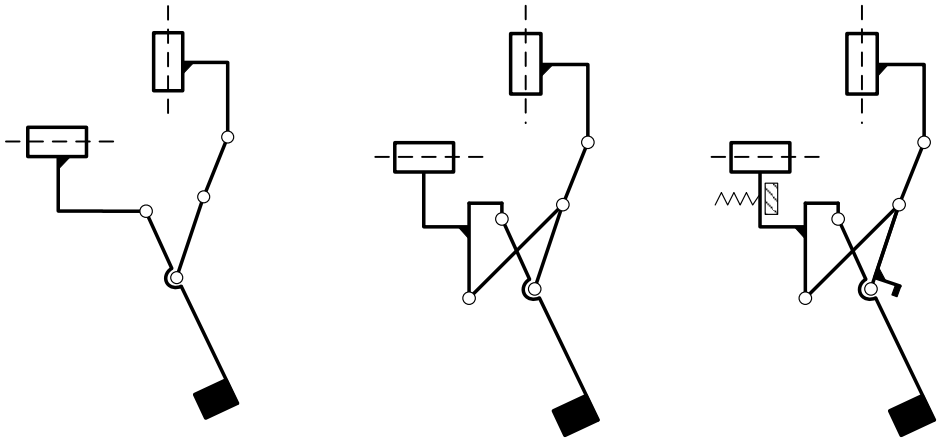

(a) Original metamorphic mechanism (b) Reducing redundant DOF (c)Adding External constraint

Fig.2. The modifying process of original metamorphic mechanism.

The metamorphic process of the vertical rolling mechanism is shown in Fig.3. In the source mechanism state (Fig.3. (a)), the spring constraint limits the horizontal

movement of the vertical roll. The source mechanism turned into the first working-phase mechanism (Fig.3. (b)). As the motor drives the screw, the slider moves downward, as shown by the dotted arrow. When it reaches the locking position of the four-bar linkage mechanism (Fig.3. (c)), the rigid constraint limits the rotation of the bars. The whole mechanism changes into a 0-DOF mechanism in an instant. When the slider continuous moving, the spring constraint get released by the driven force of the slider (Fig.3. (d)). The four-bar linkage mechanism in the dashed frame is equivalent to one link rod (Fig.3. (e)). The metamorphic mechanism changes into the second working-phase mechanism.

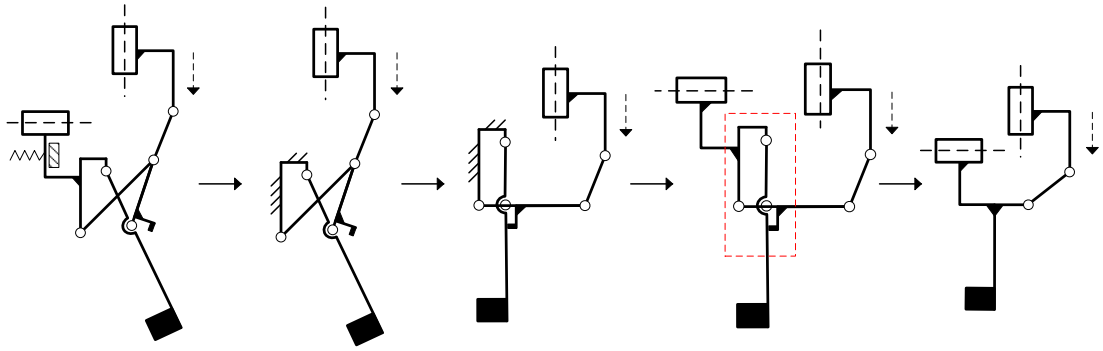

(a) (b) (c) (d) (e)

Fig.3. The metamorphic process of the vertical rolling mechanism.

4. 3D model and mechanical device of the metamorphic rolling mechanism.

From the biological and topological model shown in Fig.3, 3D model of the source-metamorphic vertical rolling mechanism is established. Added by a horizontal-roll mechanism and a fixture of welding torch, the final metamorphic rolling mechanism is modeled by Pro/E software. The 3D model and mechanical structure are shown in Fig.4 and Fig.5 respectively.

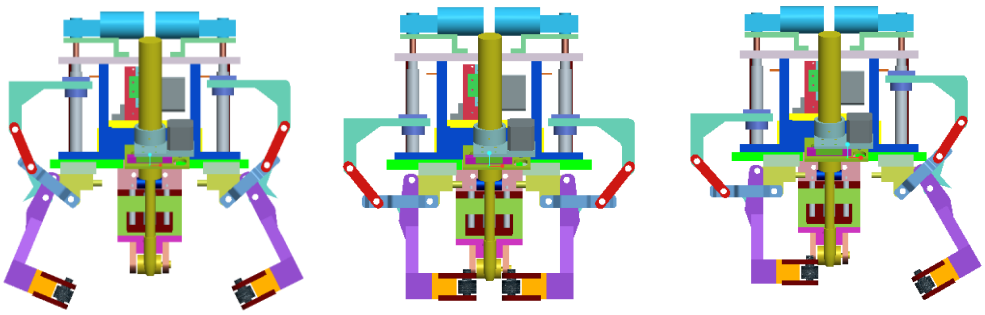

(a) (b) (c)

Fig.4. 3D model of metamorphic rolling mechanism in the three working phases of the vertical rolls.

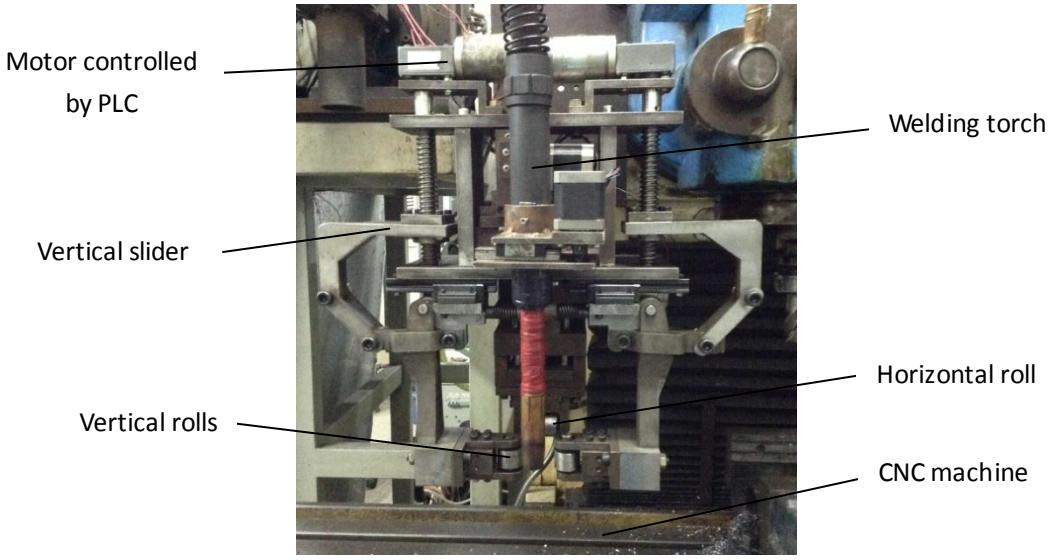

Fig.5. Mechanical structure of metamorphic rolling mechanism and the distance range of the vertical rolls.

Structure analysis and D-H equation of the metamorphic rolling mechanism

To obtain the relationship of the distance between two vertical rolls and the position of the vertical sliders linked to the screw driven by the motors (D-H equation), kinematics equations and the transformation matrices of metamorphic rolling mechanism are analyzed. The coordinate system of metamorphic vertical rolling mechanism is shown in Fig.6. According to the kinematics equations of planar mechanism，the horizontal position of vertical roll y_4 and the vertical position of the slider d can be obtained by the Homogeneous transformation matrices as Eq. (5) and Eq. (6).

$$p_4 = \mathrm{T}_3 \bullet p_0 \tag{5}$$

$$\mathrm{T}_3 = Trans(d,0,0) \bullet Rot(z_0,\theta_1) \bullet Trans(l_1,0,0) \bullet \mathrm{Rot}(z_0,\theta_2) \bullet Trans(l_2,0,0) \bullet \mathrm{Rot}(z_0,\theta_3)$$

$$= \begin{bmatrix} 1 & 0 & 0 & d \\ 0 & 1 & 0 & 0 \\ 0 & 0 & 1 & 0 \\ 0 & 0 & 0 & 1 \end{bmatrix} \bullet \begin{bmatrix} c\theta_1 & -s\theta_1 & 0 & 0 \\ s\theta_1 & c\theta_1 & 0 & 0 \\ 0 & 0 & 1 & 0 \\ 0 & 0 & 0 & 1 \end{bmatrix} \bullet \begin{bmatrix} 1 & 0 & 0 & l_1 \\ 0 & 1 & 0 & 0 \\ 0 & 0 & 1 & 0 \\ 0 & 0 & 0 & 1 \end{bmatrix} \bullet \begin{bmatrix} c\theta_2 & -s\theta_2 & 0 & 0 \\ s\theta_2 & c\theta_2 & 0 & 0 \\ 0 & 0 & 1 & 0 \\ 0 & 0 & 0 & 1 \end{bmatrix} \bullet \begin{bmatrix} 1 & 0 & 0 & l_2 \\ 0 & 1 & 0 & 0 \\ 0 & 0 & 1 & 0 \\ 0 & 0 & 0 & 1 \end{bmatrix} \bullet \begin{bmatrix} c\theta_3 & -s\theta_3 & 0 & 0 \\ s\theta_3 & c\theta_3 & 0 & 0 \\ 0 & 0 & 1 & 0 \\ 0 & 0 & 0 & 1 \end{bmatrix} \tag{6}$$

$$= \begin{bmatrix} c_{123} & -s_{123} & 0 & d + l_1 c_1 + l_2 c_{12} \\ s_{123} & c_{123} & 0 & l_1 s_1 + l_2 s_{12} \\ 0 & 0 & 1 & 0 \\ 0 & 0 & 0 & 1 \end{bmatrix}$$

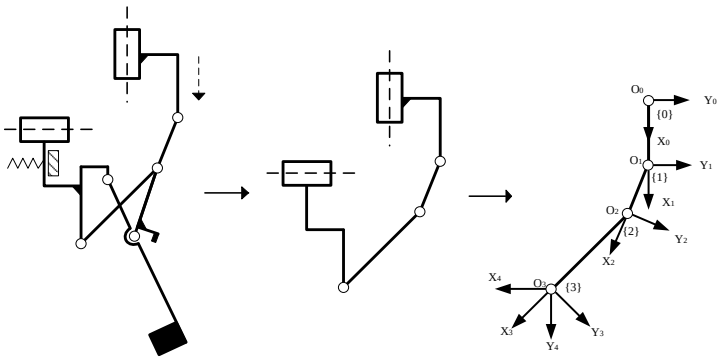

Fig.6. The coordinate system of metamorphic vertical rolling mechanism

When the metamorphic rolling mechanism works in the second working phase (Fig.3. (d)), the lengths of connecting rods and the angles of rotation satisfy the constraint equation:

$$\begin{cases} \theta_1 + \theta_2 = 90^\circ \\ \theta_3 = 0^\circ \\ p_{x_4} = c \end{cases} \tag{7}$$

Substitute Eq. (6) and Eq. (7) into Eq. (5), the horizontal position of the vertical roll y_4 can be expressed as:

$$y_4 = l_2 + \sqrt{l_1^2 - (p_{x_4} - d^2)} \tag{8}$$

l_1 and l_2 represent for the lengths of connecting rod. p_{x_4} is a constant, representing for the x coordinate of the vertical roll in coordinate system 0. Eq. (8) shows the relation between the position of the horizontal slider d and the position of the vertical roll y_4. The distance between two vertical rolls is controlled by y_4, as shown in Fig.7.

(a) (b) (c)

Fig.7. The distance between two vertical rolls is 10mm (a), 5mm (b) and 0mm (c).

Experiments

The experimental installation consists of an arc-based welding machine, a three-axis CNC machine, the designed metamorphic rolling mechanism and a PLC for the rolling mechanism motion control and data acquisition. The NC programs

generated by software are used to control the CNC machine movement. Besides, some auxiliary instructions are inserted into the NC programs including the arc striking or arc extinguishing to complete sequential control of the deposition and rolling process. By doing this, the hybrid manufacturing process is controlled automatically. Welding material and deposition parameters are shown in Table.1.

Table 1

Welding materials and deposition parameters

Materials	low alloy wire	45# steel wire
Diameter(mm)	1.6	1.2
Wire feed(m/min)	3.5	10
Peak voltage(V)	29	
Base current(A)	90	76

1. Using 1.6mm diameter low alloy wire as welding material, single beads were deposited by moving the welding torch along a straight line. The distance of vertical rolls is 8mm. The influence of vertical rolls on the bead relative deformation and surface configurations was studied. Freeform and rolled beads are deposited respectively for comparison. A numerical control rotary table is added to the installation to ensure the 180° rotation of the deposited bead. The results of the deposited beads are shown in Fig.8. Wall thicknesses of 7 points evenly along the bead are measured, as shown in Table 2 and Fig.9.

(a)

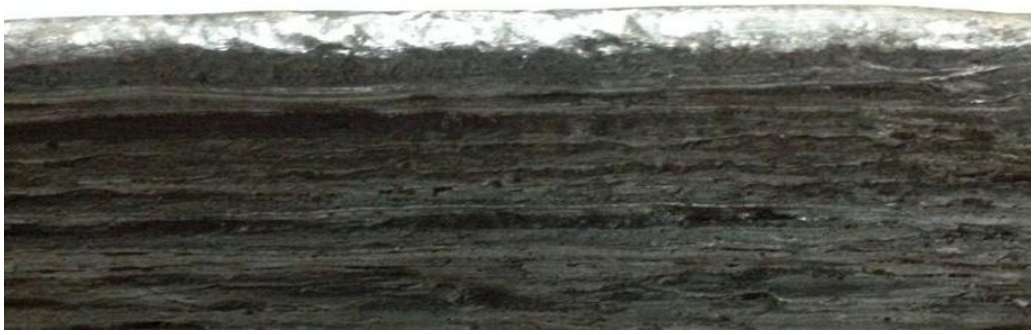

(b)

Fig.8. Lateral surface configurations of freeform (a) and rolled (b) bead.

Table2

Comparison of freeform and rolled thicknesses of the weld beads

layer No.	d1	d2	d3	d4	d5	d6	d7	Mean Value	Maximum Absolute Error	Mean Absolute Deviation	Mean Square Error
				(mm)						(mm)	
1*	9.32	8.10	8.62	8.20	8.69	8.80	10.77	8.93	2.67	0.6380	0.9065
2*	9.84	9.16	9.10	8.54	9.56	8.68	8.70	9.08	1.30	0.3796	0.4849
3	8.63	8.88	7.98	8.36	8.17	8.64	8.04	8.39	0.90	0.2837	0.3416
4	8.55	8.23	8.16	7.84	8.22	8.26	8.34	8.23	0.71	0.1331	0.2131
5	8.18	8.31	8.17	8.14	8.31	8.34	8.35	8.26	0.21	0.0804	0.0898
6	8.63	8.29	8.22	8.35	8.20	8.06	8.07	8.26	0.57	0.1400	0.1946
7	8.47	8.06	7.62	7.82	8.07	8.25	8.46	8.11	0.85	0.2453	0.3162
8	8.61	8.37	8.23	8.14	8.32	8.32	8.19	8.31	0.47	0.1069	0.1546
9	8.10	8.03	8.13	8.04	8.11	8.04	8.17	8.09	0.14	0.0445	0.0534
10	8.35	8.41	8.47	8.01	8.27	8.12	8.59	8.32	0.58	0.1576	0.2012
11	8.41	8.33	8.32	8.50	8.32	8.08	8.09	8.29	0.42	0.1188	0.1560
12	8.28	8.16	8.14	8.19	8.12	8.06	8.11	8.15	0.22	0.0502	0.0699
13	8.12	7.94	8.02	8.06	8.05	7.95	7.98	8.02	0.18	0.0518	0.0650

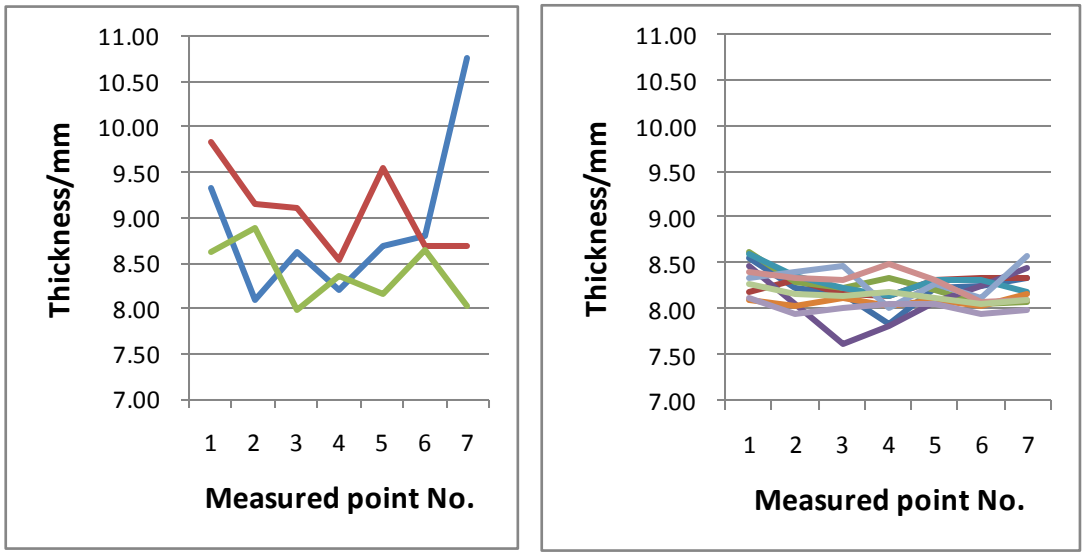

(a) (b)

Fig.9. Distribution of thickness along the freeform (a) and rolled (b) beads.

Results show that the thicknesses of rolled beads become more even than that of the freeform deposited beads. Maximum absolute error is about 78.1% lessen while that of mean absolute deviation and mean square error is about 77.8% and 78.2%. The data is acquired by dividing the average value of the thicknesses of rolled beads by those of freeform ones.

2. Using 1.6mm diameter low alloy wire as welding material, single beads were deposited by moving the welding torch along a straight line. To obtain components with various-wall thickness, the distance of vertical rolls is controlled by a

self-developed sequential-control-based ladder diagram written in PLC. The diagrammatic sketch of deposition process is shown in Fig.10. The bead is deposited with half freeform and half rolled. The numerical control rotary table in experiment 1 is added to the installation to ensure the 180° rotation of the deposited bead. Wall thickness along the bead is measured. The results of the deposited beads are shown in Fig.11. Wall thicknesses of 8 points evenly along the beads rolled are measured, as shown in Table 3. Three distances of the vertical rolls are tested.

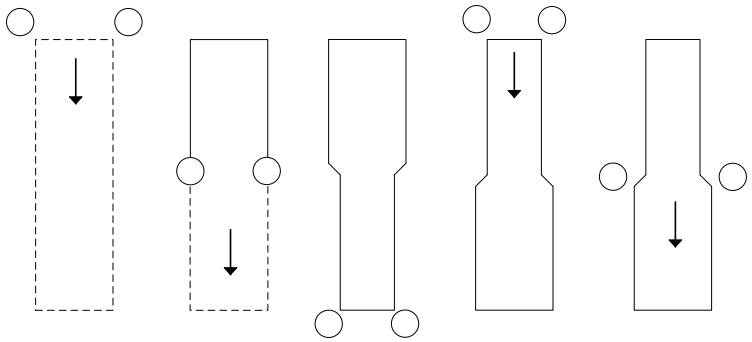

Fig.10. The diagrammatic sketch of deposition process in Experiment 2.

Table3

Comparison of half freeform and half rolled thicknesses of the weld beads

Bead No.	Distance of vertical rolls (mm)	d1	d2	d3	d4	d5	d6	d7	d8
		(mm)							
1	6	10.37	9.66	10.16	10.14	6.20	6.19	6.18	6.20
2	7.5	9.64	8.99	9.34	9.61	7.43	7.76	7.50	7.99
3	9	11.00	11.83	10.00	11.20	9.33	9.02	9.33	9.40

Fig.11. Surface configurations of half freeform and half rolled beads in the case the distance of vertical rolls is 6mm.

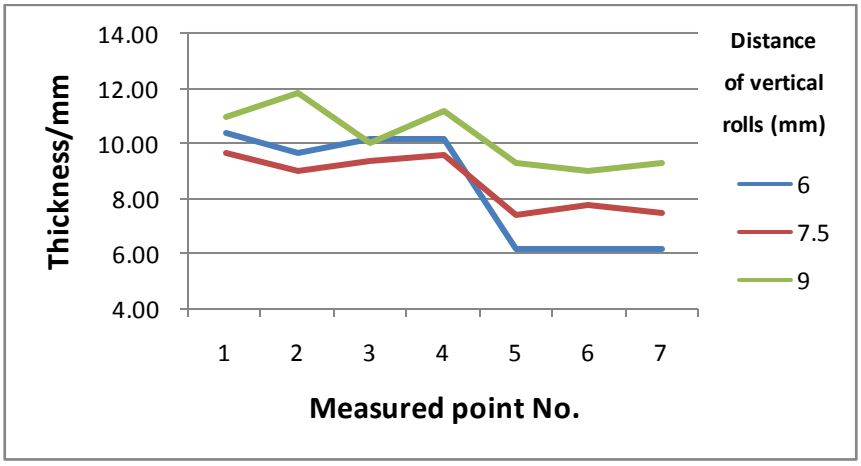

Fig.12. Thickness distributions of half freeform and half rolled beads.

Fig.12 shows the thickness distributions of half freeform and half rolled beads. The rolled parts of the beads are significantly flatter and narrower. About 40% relative deformation can be fulfilled when the distance of vertical rolls is 6mm (blue line).

3. Using 1.2mm diameter 45# steel wire as welding material, single beads were deposited on 12mm-wide substrates, freeform or rolled. The distance of vertical rolls is controlled by another self-developed sequential-control-based ladder diagram written in PLC. The diagrammatic sketch of deposition process is shown in Fig.13. The bead is deposited with middle rolled and rest freeform. Wall thickness along the bead is measured. The results of the deposited beads are shown in Fig.14. Wall thicknesses of middle and both sides of the bead is measured, as shown in Table 4 and Fig.15

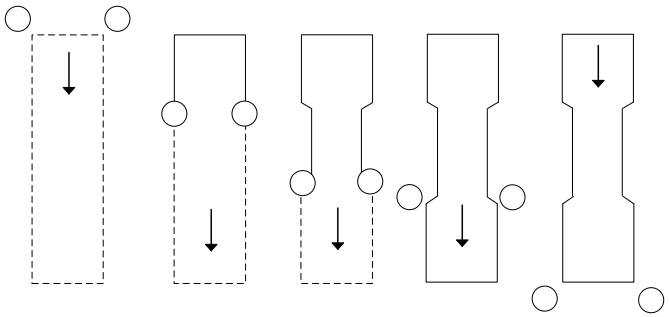

Fig.13 The diagrammatic sketch of deposition process in Experiment 3.

Table 4

Comparison of thicknesses of middle-rolled and all-freeform beads

Layer No.	d1	d2	d3	d1*	d2*	d3*
	(mm)					
1	11.70	8.58	11.03	9.84	9.80	10.35
2	11.90	8.54	11.38	9.99	9.79	10.72
3	11.93	8.57	11.99	10.25	9.81	10.95
4	12.03	8.57	10.04	10.95	9.53	10.20
5	12.22	8.45	11.08	10.35	9.14	9.98
6	11.91	8.51	11.27	10.86	9.57	10.13

The d* presents the all-freeform deposited bead sample.

Fig.14. Surface configurations of middle-rolled beads in Experiment 3.

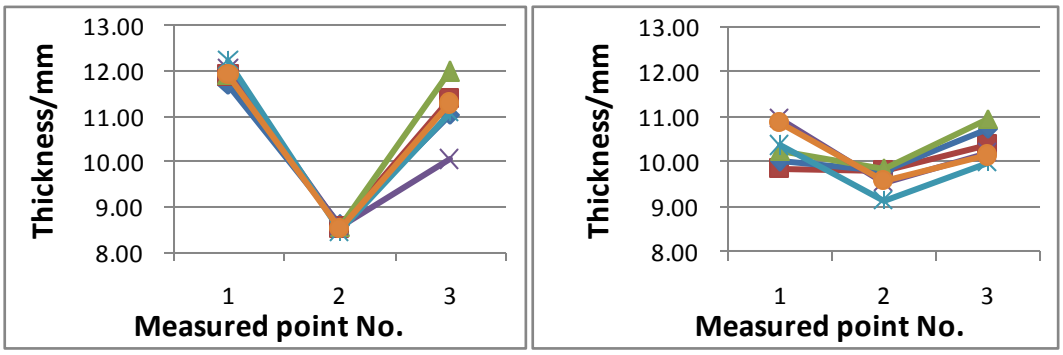

(a) (b)

Fig.15. Thickness distributions of middle-rolled (a) and all-freeform (b) beads.

Comparison shows that the middle of the rolled bead becomes 3mm thinner than both sides while that of the all-freeform bead is 1mm because of the process characteristics of welding. The thickness distribution along the horizontal direction of the middle-rolled bead is more approximate than that of the all-freeform bead.

Conclusion

This paper proposed a novel metamorphic rolling mechanism based on a developed genetic evolution synthesis that realized multiway, multiple-DOF and synchronous plastic forming in arc based deposition processing of components with variable wall thickness.

(1) A developed genetic evolution synthesis operator U^X is first proposed. U^X results in a working-phase mechanism ${}^{X}M$ from source kinematic pair b_i and executive kinematic pair b_j, providing a feasible method for metamorphic mechanism design. Using the operator, a novel metamorphic rolling mechanism is designed. The designed metamorphic mech anism makes two independent motors be capable of controlling 4 DOF of two vertical rolls and ensuring the stiffness of the mechanism by taking advantage of four-bar linkage mechanism and its locking-position characteristic. The metamorphic mechanism is energy-and-space-saving. Topology and mechanical structure and metamorphic process of the metamorphic mechanism are presented.

(2) To obtain the relationship of the distance between two vertical rolls and the position of the vertical sliders linked to the screw driven by the motors, kinematics equations and the transformation matrices of metamorphic rolling mechanism are analyzed. The D-H equation is derived, simplifying the control of the metamorphic mechanism.

(3) Three different groups of experiments are carried out. The experimental installation consists of an arc-based welding machine, a three-axis CNC machine, the designed metamorphic rolling mechanism, a PLC and an optional numerical control

rotary table. The influence of vertical rolls on the bead relative deformation and surface configurations is studied. Results show that compared with existing freeform deposition process, the bead deposited by hybrid deposition and rolling have flatter and width-controllable surfaces. Maximum absolute error of the thicknesses is about 78.1% lessen while that of mean absolute deviation and mean square error is about 77.8% and 78.2% for constant-width rolling. In the deposition of variable wall thickness bead, about 40% relative deformation can be fulfilled when the distance of vertical rolls is 6mm. In experiment 3, comparison shows that the middle of the rolled bead becomes 3mm thinner than both sides while that of the all-freeform bead is 1mm because of the process characteristics of welding.

Acknowledgments

The authors would like to give their gratitude to Youheng Fu, Yuan Xu and Shangyong Tang for their technical support. This work was financially supported by the National Natural Science Foundation of China under Project No. 51175203.

References

[1] DAI J S, REES J J., Mobility in metamorphic mechanisms of foldable/erectable kinds. Transactions of ASME, Journal of Mechanical Design, 1999, 121(3):375-382.

[2] Zhang, K., Dai, J. S., & Fang, Y. (2010). Topology and constraint analysis of phase change in the metamorphic chain and its evolved mechanism. Journal of Mechanical Design, 132(12), 121001.

[3] Zhang, H., Ruia, D., Xiea, Y., & Wangb, G. Study on Metamorphic Rolling Mechanism for Metal Hybrid Additive Manufacturing.

[4] K.P. Karunakaran, S.Suryakumar, VishalPushpa, et al., Low cost integration of additive and subtractive processes for hybrid layered manufacturing. Robotics and Computer-Integrated Manufacturing. 2010 ,26(5):490-499.

[5] Anzalone, G., Zhang, C.Long., Wijnen, B., Sanders, P., & Pearce, J. (2013). A Low-Cost Open-Source Metal 3-D Printer.

[6] Gunaraj, V., & Murugan, N. (1999). Application of response surface methodology for predicting weld bead quality in submerged arc welding of pipes. Journal of Materials Processing Technology, 88(1), 266-275.

[7] Zhang, H., Xu, J., & Wang, G. (2002). Fundamental study on plasma deposition manufacturing. Surface and Coatings Technology, 171(1), 112-118.

[8] Zhang, H., Xiea, Y., Ruia, D., & Wangb, G. HYBRID DEPOSITION AND MICRO ROLLING MANUFACTURING METHOD OF METALLIC PARTS.

[9] Srimath, N., & Murugan, N. (2012). Development of mathematical models for prediction of weld bead geometry in cladding mild steel valve seat rings by PTAW. Procedia Engineering, 38, 15-20.

[10] Cao, Y., Zhu, S., Liang, X., & Wang, W. (2011). Overlapping model of beads and curve fitting of bead section for rapid manufacturing by robotic MAG welding process. Robotics and Computer-Integrated Manufacturing, 27(3), 641-645.

[11] Chou, K. (2013, April). Process Modeling for Powder-Based Electron Beam Additive Manufacturing Technology. In 24th Advanced Aerospace Materials and Processes (AeroMat) Conference and Exposition. Asm.

[12] Aghasafari, P., Abdi, H., & Salimi, M. (2014). Artificial Neural Network Modeling of Flow Stress in Hot Rolling. ISIJ International, 54(4), 872-879.

[13] Homar, D., Kopač, J., & Dolinšek, S. (2013). Additive manufacturing and high speed cutting included in hybrid manufacturing. Journal of Production Engineering, 16(1), 5-8.

[14] Xiong, J., Zhang, G., Hu, J., & Wu, L. (2014). Bead geometry prediction for robotic GMAW-based rapid manufacturing through a neural network and a second-order regression analysis. Journal of Intelligent Manufacturing, 25(1), 157-163.

[15] Suryakumar, S., Karunakaran, K. P., Bernard, A., Chandrasekhar, U., Raghavender, N., & Sharma, D. (2011). Weld bead modeling and process optimization in Hybrid Layered Manufacturing. Computer-Aided Design, 43(4), 331-344.

[16] Duanling Li, Zhonghai Zhang, J. Michael McCarthy, A constraint graph representation of metamorphic linkages. Mechanism and Machine Theory, 2011, 46:228-238.

[17] Zhuang LI, Di WU, Wei LÜ, Effects of Rolling and Cooling Conditions on Microstructure and Mechanical Properties of Low Carbon Cold Heading Steel. Journal of Iron and Steel Research, International, 2012, 19 (11):64-70.